

OFFICIAL FILE COPY

AMMRC TR 82-48

ADA 123695

U.S. Army Materiel Research and Development Center
Watertown, Massachusetts 02172
Distribution Statement: Approved for Public Release

ADIABATIC DEFORMATION AND STRAIN LOCALIZATION

GREGORY B. OLSON, JOHN F. MESCALL, and
MORRIS AZRIN

August 1982

Approved for public release; distribution unlimited.

ARMY MATERIALS AND MECHANICS RESEARCH CENTER
Watertown, Massachusetts 02172

OFFICIAL FILE COPY

The findings in this report are not to be construed as an official Department of the Army position, unless so designated by other authorized documents.

Mention of any trade names or manufacturers in this report shall not be construed as advertising nor as an official indorsement or approval of such products or companies by the United States Government.

DISPOSITION INSTRUCTIONS

Destroy this report when it is no longer needed.
Do not return it to the originator.

Block No. 20

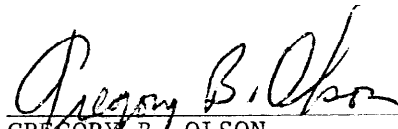
ABSTRACT

The strain localization phenomenon of "adiabatic shear" is generally attributed to a plastic instability arising from a thermal softening effect during adiabatic or near-adiabatic plastic deformation. High strain-rate adiabatic torsion tests indicate that the effective shear stress-strain ($\bar{\tau} - \bar{\gamma}$) relations for high-strength (rate-insensitive) steels can be described by a simple expression of the form:

$$\bar{\tau} = \bar{\tau}_0 (1 + \alpha \bar{\gamma}) \exp(-\beta \bar{\gamma})$$

where $\bar{\tau}_0$ is a constant, α and β are dimensionless hardening and softening parameters. The flow stress reaches a maximum at an instability strain, $\bar{\gamma}_i = \beta^{-1} - \alpha^{-1}$. With parameters derived from the torsion tests, this relation has been used in computer simulations of the development of intense shear localization in a simple uniformly loaded body. Strain localization has been studied under conditions of both quasistatic and dynamic deformation. Application to the simulation of ballistic penetration is in progress.

Experimental evidence indicates the existence of a pressure-dependent strain softening effect attributed to subcritical shear microcracks which contributes to shear instability in mild steels. This phenomenon may also operate in high-strength steels, giving rise to a pressure-dependent β parameter. Experiments are being designed to determine the relative importance of this effect in the adiabatic deformation of high-strength steels and its possible role in ballistic penetration.

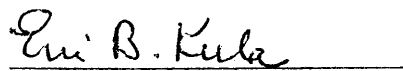

 GREGORY B. OLSON
 Research Metallurgist

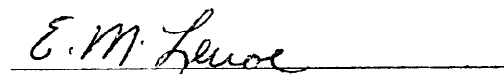

 MORRIS AZRIN
 Supervisory Metallurgist

APPROVED:


 JOHN F. MESCALL
 Supervisory Mechanical Engineer

APPROVED:


 E. B. KULA
 Chief
 Metals Research Division


 E. M. LENO
 Acting Chief
 Engineering Mechanics Division

CONTENTS

	Page
INTRODUCTION.	1
BACKGROUND.	1
ADIABATIC FLOW RELATIONS.	4
COMPUTER SIMULATION OF SHEAR LOCALIZATION	6
APPLICATION TO BALLISTIC PENETRATION.	8
PRESSURE-DEPENDENT SHEAR INSTABILITY.	9
CONCLUSION.	11
APPENDIX. ADIABATIC STRESS-STRAIN RELATIONS.	21
ACKNOWLEDGMENTS	24
LITERATURE CITED.	25

INTRODUCTION

Since the classic work of Zener and Hollomon,¹ it has been well recognized that the temperature rise accompanying plastic deformation under conditions of restricted heat transfer can contribute a destabilizing strain-softening contribution to plastic flow behavior. The associated strain localization phenomenon of "adiabatic shear" is known to play an important role in the dynamic plastic deformation encountered in such diverse areas as machining, metalworking, cryogenics, ballistic penetration, and explosive fragmentation. The conventional view is that the phenomenon can be treated as a continuum plastic instability, provided that the constitutive flow behavior is properly described. We will here examine appropriate constitutive relations for plastic flow under adiabatic conditions, and assess the use of these relations in computer codes allowing an extension from the familiar regime of quasistatic plastic flow to a treatment of strain localization during fully dynamic plastic deformation. With the ultimate objective of understanding and controlling the ballistic penetration of high-strength steels, we will focus largely on the behavior of steels with emphasis on the conditions for the initiation of flow localization.

BACKGROUND

The phenomenon of adiabatic shear as it occurs in ballistic penetration is illustrated in Figure 1.² Figure 1a shows the extensive plastic deformation that occurs when a hard steel projectile impacts a low-strength steel target. As the strength of the target is increased, eventually the localized deformation mode of Figure 1b occurs, in which plastic flow is concentrated in thin shear bands which appear white after metallographic etching. The localized flow results in a "shear plugging" mode of target failure in which the material ahead of the projectile is ejected as one solid piece with relatively little attendant energy absorption. This tendency for flow localization at high strength levels is also important in the behavior of projectiles. A mixture of fracture and white band formation can be noted in the projectile shown in Figure 1a.

Recent reviews of the subject of adiabatic deformation and flow localization are listed in Table 1. The reviews of Rogers^{3,4} and Bedford et al.,⁵ give an excellent overview of the general phenomenon including the microstructures resulting from localized flow. The continuum plasticity theory of adiabatic flow localization is treated by Clifton,⁶ and a general survey of strain localization, including adiabatic shear, is given by Argon.⁷ A concise treatment of the specific role of adiabatic shear in armaments and ballistics can be found in the review of Samuels and Lamborn.⁸ Table 1 also lists experimental measurements relevant to the constitutive relations for adiabatic plastic flow⁹⁻¹⁵ which will be discussed later.

Much attention has been directed to the microstructures of the white-etching bands formed in high-strength steels.^{3,8,16-18} The bands are generally found to be composed of very fine-grained ferrite supersaturated with carbon.¹⁶ As similar microstructures are developed during cyclic deformation of bearing steels and the wear of surfaces¹⁹⁻²¹ where substantial temperature rises are less likely, the relative importance of temperature and high plastic strain in the development of these bands is not clear. It should be noted that these white-etching bands ("transformation bands") as distinct from simply bands of concentrated strain ("deformation bands")²² represent an advanced stage of the localized flow process. Mechanisms contributing to the development of the white-band microstructures are not necessarily relevant to the conditions for the "onset" of the plastic flow localization. For example, the experimentally observed conditions for the onset of instability in high-strength steels to be discussed later

Table 1. REVIEWS OF ADIABATIC DEFORMATION AND LOCALIZATION

Rogers 1979 (3,4)	
Bedford et al. 1974 (5)	General phenomenology
Clifton 1978 (6)	Analysis of shear localization
Argon 1973 (7)	General theory of stability and localization
Samuels and Lamborn 1978 (8)	Role in armaments and ballistics
<hr/> Shear Stress-Strain Measurements - Steels <hr/>	
Culver 1973 (9)	
Costin et al. 1979 (10)	Adiabatic torsion, mild steel
Lindholm and Hargreaves 1976 (11,12)	Adiabatic torsion, high strength steel
Walker and Shaw 1969 (13)	Isothermal shear and compression, mild steel
Luong 1977 (14, 15)	Adiabatic shear and compression, mild steel

would be accompanied by a maximum temperature rise of 50°C. Such processes as martensite-austenite reversion,¹⁶⁻²³ often invoked in reference to white-band formation, are of little relevance to the initiation of localization at such low temperature. From a practical standpoint, it would seem that the most fruitful approach to the control of the adiabatic shear phenomenon would be to delay the onset of localization rather than to search for possible mechanisms of restabilization after intense localization has already occurred.

Continuum plasticity analyses of the onset of strain localization under adiabatic or near-adiabatic conditions generally ascribe the chief destabilizing influence to a strain softening term given by:

$$\frac{\partial T}{\partial \gamma} \frac{\partial \tau}{\partial T},$$

with τ the shear flow stress, γ the plastic shear strain, and T the temperature.²⁴ This term, often referred to as "thermal softening," is a negative quantity due to the negative temperature dependence of τ . For fully adiabatic conditions, under which a fraction, f , of the work of plastic deformation, $\tau d\gamma$, is not stored as structural defects and therefore contributes to a temperature rise, the term becomes:

$$\frac{\partial T}{\partial \gamma} \frac{\partial \tau}{\partial T} = \frac{f\tau}{\rho C_p} \frac{\partial \tau}{\partial T}, \quad (1)$$

where ρ and C_p are the density and specific heat. The proportionality with τ is the principal reason why the thermal effect becomes more important in higher strength materials. If this term becomes large enough to bring the net strain-hardening rate to zero

$$\frac{d\tau}{d\gamma} = 0, \quad (2)$$

deformation in shear becomes unstable, and localization of flow will occur. Analytical treatments of the growth of flow perturbations using elaborate constitutive models have indicated situations where flow can localize in shear while $d\tau/d\gamma$ is still slightly positive, but for the most part Eq. 2 represents a reasonably useful criterion for the onset of shear localization in the regime of quasistatic plastic flow.

The perturbation analyses show that heat transfer from a deforming volume, through reduction of $\partial T/\partial \gamma$, can exert a stabilizing influence on plastic deformation similar to the effect of strain-rate hardening in superplastic flow. Application of a one-dimensional heat flow solution²⁵ for a constant rate of heat input into a region of characteristic dimension L , as discussed by Culver,^{9,26} provides a useful basis for assessing the importance of heat flow during plastic deformation at high strain rates. The temperature profile at time t is controlled by the parameter $L^2/\kappa t$, where κ is the thermal diffusivity. A rough boundary between the regimes of "isothermal" and "adiabatic" behavior is

$$\frac{L^2}{\kappa t} \approx 1. \quad (3)$$

The average temperature within the region defined by L will be 10% and 90% of the fully adiabatic limit for values of $L^2/\kappa t$ of $\sim 10^{-2}$ and $\sim 10^2$. At a constant strain rate $\dot{\gamma}$, time can be expressed as $t = \gamma/\dot{\gamma}$. Use of an appropriate value of κ for steels indicates that for most of the conditions for which "adiabatic shear banding" is observed, the deformation preceding localization is very nearly fully adiabatic, and heat transfer becomes important only after intense localization has occurred. This is particularly so in the case of ballistic penetration. One can in fact use the assumption that restricted heat flow is necessary to the development of white-etching shear bands as a means to calculate a lower limit to band thickness. For local strain rates of 10^5 to 10^6 s^{-1} and local strains of 1 to 10, adopting Eq. 3 as a criterion for significant heat transfer gives a band dimension L of the order of $10 \mu\text{m}$ in agreement with the white band thicknesses observed in steels.^{22,23,27-29}

The analytical treatments of strain localization further indicate that the most important stabilizing influence is the intrinsic structural strain hardening rate (as determined for example from the isothermal flow behavior).³⁰ This is perhaps the parameter most amenable to manipulation in attempting to delay the adiabatic instability. Most analyses conclude that strain-rate hardening is also a stabilizing influence,³¹ although Clifton⁶ concludes the opposite; the physical basis of this result is not obvious. For high strength steels, however, strain-rate sensitivity is small and its influence can be reasonably neglected.

Estimates of critical strains for adiabatic instability have been made based on constitutive relations (largely empirical) developed originally for isothermal deformation, and compared with results of high strain-rate torsion tests.⁹⁻¹² Conclusions regarding agreement between theory and experiment are mixed.

The flow localization analyses discussed thus far have been based on quasistatic deformation theory. To extend the localization concepts into the regime of dynamic plastic deformation, as is appropriate for problems like ballistic penetration, the concept of "wave trapping" has been proposed.³² In essence, this concept is based on the velocity of a plastic shear wave, v_p^s , expressed by:

$$v_p^s = \sqrt{\frac{1}{\rho} \frac{d\tau}{d\gamma}} . \quad (4)$$

When the net strain hardening rate reaches zero (as in Eq. 2), the plastic wave should cease to propagate, and deformation should localize. This concept will be commented on further when results of dynamic computer code calculations are discussed.

ADIABATIC FLOW RELATIONS

While the temperature T is constant during an isothermal process, the entropy S is the thermodynamic state function which is constant under adiabatic conditions. From the viewpoint of thermodynamics and statistical mechanics, temperature and entropy are equally fundamental quantities, and an equation of state can be formulated with either as an independent variable. Hence, instead of attempting to apply empirical constitutive relations based on isothermal experiments to the case of adiabatic deformation, it is equally valid to formulate new empirical constitutive relations for adiabatic (isentropic) plastic flow derived directly from experiments performed under adiabatic conditions. One should note that since the temperature is a single-valued function of the state variables under adiabatic conditions, it is no more necessary to determine the temperature during adiabatic deformation than it is to determine the entropy during isothermal deformation, for purposes of describing constitutive flow behavior.

An area where an adiabatic formulation for plastic flow should be particularly useful is in computer codes designed to treat dynamic deformation involving plastic wave propagation. Constitutive relations so far employed in these codes have generally involved either ideal plastic or isothermal work hardening behavior.² Even in conditions of highly localized flow, the assumption of adiabatic conditions should be a significant improvement over the isothermal assumption, particularly when deformation times are in the microsecond range.

Based on the usual physical assumptions applied to adiabatic plastic deformation, possible anticipated forms for $\tau - \gamma$ relations under constant $\dot{\gamma}$ adiabatic conditions are derived in the Appendix. Of these possibilities, an expression which is found to fit the results of adiabatic deformation experiments particularly well is given by:

$$\bar{\tau} = \bar{\tau}_0 (1 + \alpha \bar{\gamma}) \exp(-\beta \bar{\gamma}) . \quad (5)$$

Here $\bar{\tau}_0$ is a constant representing the shear yield stress, α is a dimensionless hardening parameter, and β is a dimensionless softening parameter which can be interpreted in terms of the thermal effect represented in Equation 1. In order to generalize to different stress states, $\bar{\tau}$ and $\bar{\gamma}$ here represent "effective" or "equivalent" shear stress and shear strain based on a Von Mises or "J₂" flow criterion.

The $\bar{\tau} - \bar{\gamma}$ behavior given by Eq. 5 is depicted schematically in Figure 2. The true stress is seen to reach a maximum at a shear instability strain, $\bar{\gamma}_i$, which is simply determined by the α and β parameters:

$$\bar{\gamma}_i = \beta^{-1} - \alpha^{-1}. \quad (6)$$

Reliable direct measurements of adiabatic plastic flow behavior can be obtained from torsion and simple shear tests in a relatively narrow range of experimental conditions defined by material properties. The strain-rate must be sufficiently high that conditions are reasonably adiabatic, yet sufficiently low that deformation is not dominated by plastic wave propagation, such that stress and strain can no longer be simply inferred from load-displacement information. The boundary between isothermal and adiabatic regimes is expressed in Eq. 3. An approximate boundary between the regimes of "quasistatic" and "dynamic" plastic flow in shear deformation is given by the condition that the imposed boundary velocity v_0 produce an initial elastic stress pulse equal to the material flow stress τ_0 . This is expressed by

$$v_0 = \frac{\tau_0}{\rho v_e^s} \quad (7)$$

where v_e^s is the elastic shear wave velocity given by $v_e^s = \sqrt{G/\rho}$ with G the elastic shear modulus. From Eq. 3 and 7 the range of nominal strain rates corresponding to the regime of "quasistatic adiabatic flow" is given by

$$\frac{\kappa}{L^2} < \dot{\gamma} < \frac{\tau_0}{L\sqrt{\rho G}}. \quad (8)$$

Provided instrumental factors such as "ringing" and inertial loading effects are properly controlled, tests run on steel specimens with convenient L dimensions can fall comfortably within this range at strain rates of 10^2 to 10^3 s^{-1} . Such experiments of course represent a compromise which is neither fully adiabatic nor genuinely static, but from a practical standpoint, the thermal conditions are as close to adiabatic as a conventional "isothermal" test is to isothermal, and the character of the plastic deformation is essentially that described by the static plasticity viewpoint.

Experimental adiabatic $\tau - \gamma$ curves for steels obtained from thin-walled torsion specimens at a strain rate of 10^2 s^{-1} are shown in Figure 3. The solid curve and open point are from the data of Culver⁹ for mild steel, the open point estimated from the load and local strain (from scribe marks) at fracture. Data points from Lindholm and Hargreaves^{11,12} for quench-and-tempered HY-TUF steel in both air-melted (AM) and vacuum-arc-remelted (VAR) conditions are also shown. Results very similar to those of HY-TUF steels have been obtained for 4340 steel tempered to hardness of HRC 45.³³

The dotted curves in Figure 3 represent the fit of Eq. 5 using the parameters given in Table 2. Except for the open point for the mild steel estimated from local strain measurement, the data presented are obtained directly from load-displacement measurement as such, the points beyond the stress maximum are unreliable, since deformation becomes localized, and strain can no longer be directly inferred from the measured displacement. Conditions during localized flow will also be less adiabatic due to the smaller characteristic distance L .^{*} The deformation preceding the stress maximum, however, is found

*At constant imposed boundary velocity, the L^2 dependence of the thermal behavior is partially compensated by an L^{-1} dependence of local strain rate.

to be reasonably homogenous, and conditions are fairly close to adiabatic. The simple relation of Eq. 5 is found to fit the data quite well.

Table 2. PARAMETERS DERIVED FROM ADIABATIC TORSION DATA

	Mild Steel	HY-TUF (VAR)	HY-TUF (AM)
$\bar{\tau}_0$	31.8 ksi (219 MN/m ²)	132 ksi (910 MN/m ²)	133 ksi (917 MN/m ²)
α	2.56	2.36	7.85
β	0.667	1.61	4.18
$\bar{\gamma}_i$	1.11	0.20	0.112
$\bar{\tau}_{max}$	58.3 ksi (402 MN/m ²)	141 ksi (972 MN/m ²)	157 ksi (1082 MN/m ²)

The adiabatic $\tau - \gamma$ data of Figure 3 verify that a shear instability occurs at fairly low strains in the high strength steels, consistent with the expected greater thermal effect. Having obtained $\tau - \gamma$ relations at a strain-rate of $10^2 s^{-1}$, we can now model the development of shear localization by applying these relations in computer code calculations. We will adopt the assumption that these same relations apply at higher strain rates. For the high-strength steels which are known to be fairly strain-rate insensitive, this approximation seems particularly appropriate.

COMPUTER SIMULATION OF SHEAR LOCALIZATION

Computer simulations of adiabatic plastic deformation have been run using the HEMP code developed by Wilkins³⁴ for treating dynamic deformation. The code couples conservation laws with an appropriate equation-of-state for dynamic as well as static high pressure conditions, employing a finite-difference formulation, and integrating the equations of motion step-by-step in time. Problems can be treated which include two spatial dimensions - plane strain or those involving rotational symmetry. Virtually any elastic-plastic constitutive law can be employed.

Input to the code consists of specification of the problem geometry, appropriate initial velocities or applied stress fields, and the material dynamic flow properties. Output consists of a detailed space-time history of all important physical quantities such as stress, strain, displacement, and velocity. Thus it can be a valuable tool for providing a dynamic "whole field" analysis required to decipher the sequence of events occurring in complex dynamic problems. Numerous comparisons of HEMP code predictions with experimental results indicate excellent agreement when material properties can be adequately specified. Further details of the computational procedures can be found in Reference 2.

To treat the development of shear localization, the deformation of the simple rectangular body depicted in Figure 4 was simulated, using the plastic flow relation of Eq. 5 with parameters similar to those of the HY-TUF steel in Figure 3. The bottom surface was held stationary, and a constant velocity was applied to the top, corresponding to a constant imposed nominal strain rate. The development of shear localization is illustrated in subsequent figures representing strain profiles along the midplane AA'.

Figure 5 shows the development of the strain profiles at different times for an imposed boundary velocity of 1×10^3 cm/s. This velocity represents a lower limit for convenient calculation times using the HEMP code, and should correspond to conditions of effectively quasistatic plastic deformation. The dashed line depicts the instability strain, γ_i , and the numbers next to each strain profile represent time in microseconds. It is seen that deformation is initially fairly uniform, but once the instability strain is exceeded deformation becomes localized in accordance with the prediction of continuum plasticity theory.

Two shear bands are found to nucleate; each is only one zone in thickness. The actual positions of the shear bands are in agreement with the slip-line-field analysis of Green³⁵ for this problem. Such agreement is appropriate, since slip-line-field theory predicts the flow pattern for a material with no work-hardening capacity; this is identical to the condition which prevails at the instability strain. At later times, deformation is found to concentrate in the band near the lower stationary surface (A'). As shown in Figure 6, very nearly identical deformation behavior is found for an imposed velocity of 3×10^3 cm/s, just below the threshold of dynamic behavior expressed by Equation 7.

The deformation behavior for a velocity of 4×10^3 cm/s, just beyond this dynamic threshold, is illustrated in Figure 7. The behavior is very similar to that of the lower velocities, with the exception that the shear band near the upper (moving) surface is now the one which grows at longer times, and the band near the lower surface appears to be slightly more diffuse. This is illustrated more clearly by the behavior of the complete grid pattern with time as shown in Figure 8.

The influence of imposed strain rate on the development of flow localization at these velocities is depicted in Figure 9, which shows the maximum strain in the AA' section as a function of imposed boundary displacement, vt . As the imposed velocity is increased, the development of localization for strains beyond the instability strain is delayed with respect to boundary displacement. The influence of the zone size employed in the HEMP code simulations was examined by running the lowest velocity problem with twice the zone size. The overall deformation pattern was qualitatively the same, but as Figure 9 indicates, the intensification of strain within the shear band was significantly delayed. This effect may be partly because the strain in a zone resulting from a given relative displacement across the zone will be inversely proportional to the zone size. However, the observed difference in strain increments during localization is substantially greater than the zone size ratio. These effects suggest that, while the HEMP code results are in excellent agreement with the qualitative behavior expected in the regime of quasistatic plastic deformation, details of the localization process, such as the time scale and intensity of the localization, may be significantly influenced by the finite zone size employed in the computer code. This could potentially lead to difficulties in the simulation of some dynamic problems.

Extending the simulation well into the regime of dynamic plastic deformation, the strain profiles along AA' for an imposed velocity of 3×10^4 cm/s are shown in Figure 10. The behavior is radically different from that of Figures 5-7. Rather than a period of relatively uniform deformation followed by localization, the effect of the plastic instability is superimposed on the nonuniform deformation associated with dynamic flow. It appears that strains greater than the instability strain propagate in as far as the position where the shear band forms in the quasistatic case (again corresponding to the slip-line-field solution); there is then intense localization in the first zone at the surface, while, simultaneously, strains below the instability strain continue to propagate

The role of the plastic instability in establishing this deformation pattern is best seen by comparing this result with that of the identical problem run with monotonic work hardening behavior.* This is shown in Figure 11 and illustrates the basic non-uniformity of the dynamic plastic deformation. Note that all strains continue to propagate within the material. Comparing strain profiles at different times, the local plastic strain rate can be calculated. This is plotted as a function of position along AA' at a time of 10 μ s for the results of both the monotonic hardening and adiabatic stress-strain relations in Figure 12. The influence of the adiabatic plastic instability is quite clear. Whereas the local strain rate varies smoothly between 10^4 and 10^5s^{-1} in the monotonic hardening case, the shear localization resulting from the adiabatic stress-strain relation causes the local strain rate to approach 10^6s^{-1} in the first zone. Adjacent to this zone is a nondeforming "dead" region, followed by a region in which strains below the instability strain propagate in a manner very similar to the monotonic hardening case. A comparison of the complete grid patterns at 10 μ s for the monotonic hardening and adiabatic behavior is shown in Figure 13, emphasizing the intense localization associated with the plastic instability in the adiabatic case.

The observed dynamic plastic deformation behavior is in qualitative agreement with the notion of "plastic wave trapping" mentioned earlier. The position of contours of constant strain, $\Delta Y(\bar{\gamma})$, is plotted versus time for the adiabatic problem in Figure 14. The contour for a strain of $1/2 \bar{\gamma}_i$ propagates at a fairly constant velocity. This velocity corresponds approximately to the expected velocity of a plastic shear wave; however, lower strain contours propagate much faster, and there is evidence that other types of waves contribute to the deformation through "end effects" associated with the particular geometry chosen. The strain contours of $\bar{\gamma}_i$ and $2\bar{\gamma}_i$ do propagate a certain amount, but after 5 μ s, their velocity is seen to reach zero in accordance with the trapping concept. While the overall behavior is more complex than the simple plane wave description, and there is some propagation of strains above $\bar{\gamma}_i$, the development of inter localization and an adjacent nondeforming region does appear to be associated with the instability strain $\bar{\gamma}_i$, where $d\bar{\tau}/d\bar{\gamma}$ reaches zero.

The observed dependence of the adiabatic deformation behavior on imposed velocity is summarized in Figure 15, which depicts the complete grid patterns at comparable imposed displacements of the upper surface. At the lowest velocities, two shear bands nucleate, but the lower band grows. For an intermediate velocity at the threshold of dynamic flow, two bands nucleate, but the lower band is more diffuse, and the upper band eventually grows. At the highest velocities there is intense localization in one band at the upper surface.

For the case of a simple shear deformation, then, the use of the empirical adiabatic flow relation in the HEMP code allows us to simulate shear localization in agreement with expected behavior under quasistatic conditions, and to examine the manner in which dynamic flow conditions modify this behavior. It now becomes of interest to apply this approach to more complex problems.

APPLICATION TO BALLISTIC PENETRATION

Some preliminary calculations have been run applying the HEMP code with adiabatic flow relations to the impact of 1.0-cm-diameter steel projectiles against 1.25-cm-thick steel plates. Using the same high-strength steel flow parameters for the projectile as used in the simple shear simulations, and using the mild steel behavior of Figure 3

*Work hardening parameters appropriate to the isothermal deformation of high strength steels were used, keeping initial yield stress constant.

for the target, the deformation pattern obtained at a stage of partial penetration is shown in Figure 16. Except for details of projectile fracture which are not treated in the model, the overall behavior is in reasonable agreement with that depicted in Figure 16. Due to the high instability strain in the mild steel, shear banding in the target is not expected.

If the properties of the target are made the same as the projectile, the behavior depicted in Figure 17 is found. While there is no evidence of shear banding in the target there is severe flow localization in the projectile. Such extensive deformation of the projectile is not entirely unexpected, since at equal hardness the target has a geometrical advantage over the projectile.

In an effort to simulate shear plugging of the target, the complication of projectile deformation was removed from the problem by using an extreme flow stress for the projectile. This led to the deformation pattern depicted in Figure 18. Although these conditions would be expected in practice to lead to the plugging behavior of Figure 1b, the simulated projectile is found to burrow through the target by what appears to be a "hydrodynamic flow" mode of target deformation. While each of these simulations allowed frictionless sliding at the target-projectile interface, the addition of complete surface welding in the latter problem did not substantially alter the deformation pattern nor did the use of monotonic work hardening behavior for the target material, although the actual stress levels were influenced. It thus appears that the behavior of the simulation is essentially that of a plastically stable material. Although the instability strain is exceeded, and there is strain softening, the localization of flow in the form of shear bands is suppressed, and an alternate mode of plastic flow ensues.

The velocity and zone-size dependence of the localization process observed in the simple shear simulations implies that the development of shear bands in the ballistic penetration simulation might be delayed by the finite zones employed by the HEMP code. The role of zone size warrants further investigation, but the velocities involved in the ballistic penetration simulations are not greatly different from that of the fully dynamic simple shear simulation in which fairly intense flow localization developed in only a few microseconds.

It is important to note that the stress states encountered in ballistic penetration are radically different from that of the simple shear, involving substantial hydrostatic stresses. The simulations of the high-strength target penetration indicate a compressive hydrostatic component in the region ahead of the projectile of the order of 50 kbar (750 ksi) during gross plastic deformation. At the same time, there is a highly deformed region of the target several zones wide near the projectile corners in which a tensile hydrostatic component of ~ 10 kbar (150 ksi) is maintained; it seems very likely that local fracture would occur in this region with an attendant significant modification of the pattern of plastic flow. These factors, together with the apparent inadequacy of the simple shear description in simulating ballistic penetration by plugging, raise the interesting question of the possible interrelationships of pressure, fracture, and shear instability.

PRESSURE-DEPENDENT SHEAR INSTABILITY

Of particular concern in the modeling of the high-strain plastic flow behavior of steels are experimental observations indicating that isothermal flow behavior is also describable by the empirical relation developed for adiabatic flow (Eq. 5), and that the

instability strain γ_i is pressure dependent. Figure 19 represents the results of Walker and Shaw¹³ from plane-strain linear shear experiments in which a constant uniaxial compressive load is superimposed normal to the shear plane. The figure shows effective shear stress-strain curves at different normal stresses for a cold-worked 0.10C mild steel under isothermal conditions. A shear instability was observed at the stress maximum. As Figure 19 shows, the instability strain increases with compressive stress. Walker and Shaw interpret this result in terms of a contribution to high strain plastic flow from the propagation and rewelding of subcritical shear microcracks which introduce a pressure-dependent strain-softening effect. Bridgman³⁶ obtained similar results in combined torsion and compression tests on steels, and reported observing shear cracks which open and close during deformation. The pressure-dependent frictional sliding across shear cracks is known to be an important plastic flow mechanism in brittle materials under high pressure, and the development of shear localization for such materials has been treated quantitatively by Rudnicki and Rice.³⁷ The Walker and Shaw results for mild steels were verified in similar experiments by Luong,^{14,15} which included a quantitative scanning electron microscopy (SEM) study of the development of voids and microcracks during deformation. The defects were observed before the stress maximum and were found to increase in number with further straining. Whereas Walker and Shaw suggest that the strain-softening effect associated with microcrack formation is due to reduced effective cross-sectional area, Luong concludes that this geometric effect can account for only 10% of the observed stress drop, and suggests that local enhancement of slip around voids may be a more important softening contribution. One might also consider the kinetics of crack growth itself as a deformation mechanism with associated dynamic softening behavior analogous to the "transformation plasticity" effects encountered in strain-induced transformations and mechanical twinning.^{38,39}

Whatever the actual mechanism, it is clear from the experimental results depicted in Figure 19 that a pressure-dependent shear instability in steels exists. Analysis of the Walker and Shaw data indicates that the observed behavior can be reasonably well represented by Eq. 5 if the β softening parameter is made a linear function of pressure. Rather than a thermal softening effect, the softening is regarded here as a pressure dependent "microcrack" softening, $\beta^c(P)$ expressed by

$$\beta^c(P) = \beta_0^c - kP \quad (9)$$

with β_0^c and k constants. The associated behavior of β^c and γ_i with pressure P , and the form of the $\bar{\sigma}$ - $\bar{\gamma}$ curves for different pressures, are represented schematically in Figure 20. Beyond a critical pressure P^* there is no softening effect, and strain-hardening is monotonic.

If the pressure-dependent strain-softening effect occurs under isothermal conditions it can also be expected during adiabatic deformation. This has been verified by Luong^{14,15} by extending the shear + compression tests on mild steels to high-strain rates. Flow stresses were higher due to the rate sensitivity of the mild steels, and the shear instability occurred at lower strains, still a function of compressive stress. The simplest model of pressure-dependent behavior under adiabatic conditions is to assume that a fixed thermal softening contribution β^{th} and the pressure-dependent term $\beta^c(P)$ are additive:

$$\beta = \beta^{th} + \beta^c(P). \quad (10)$$

This gives the behavior represented schematically in Figure 21. Beyond the critical pressure P^* where $\beta^c = 0$, β becomes β^{th} and the instability strain reaches the constant value γ_1^{th} associated with the thermal softening effect alone. This gives the family of $\tau - \gamma_1$ curves depicted in Figure 21c, in which the curve for pressures above P^* shows the theoretical behavior for the thermal instability in the absence of the pressure-dependent softening contribution.

The flow behavior predicted by Eqs. 5, 9, and 10 and represented in Figure 21 provides us with a model for pressure-dependent adiabatic plastic deformation which could be applied to the computer simulation of dynamic deformation problems. While values of the parameters can be estimated from the experiments on mild steels, unfortunately no appropriate experimental information is currently available for the high-strength steels for which shear instability is of greatest interest. In order to obtain this information, an instrumented pendulum-type impact machine is being modified at AMMRC to allow testing of the double-shear specimen illustrated schematically in Figure 22. The central portion of the specimen is struck by an instrumented tup at sufficient velocity to impose adiabatic strain rates of 10^2 to $10^3 s^{-1}$ while a constant load P_n is maintained normal to the plane of shear. Should the high strength steels show the same pressure-dependent shear instability behavior found in the mild steels, a better understanding of the mechanisms underlying pressure-dependent softening will be imperative to an understanding of the phenomenon of adiabatic shear.

CONCLUSION

While all the factors underlying the shear instability observed during the adiabatic deformation of high strength steels are not well understood, the use of empirical adiabatic flow relations derived from torsion test results has allowed successful computer simulation of strain localization in a simply loaded body. The results are in excellent agreement with expected behavior under quasistatic deformation conditions and have also allowed an examination of the manner in which dynamic deformation can modify the development of flow localization. While the use of this simple flow relation in preliminary computer calculations for the more complex problem of ballistic penetration has not successfully simulated shear plugging behavior, some available experimental results indicate that incorporation of pressure-dependent softening effects may be necessary to correctly model the adiabatic flow behavior of steels under complex loading conditions. If further experiments verify that these pressure-dependent effects operate in the high strength steels, this will indicate that an understanding of the role of voids and microcracks in the high strain deformation of steels is essential to an understanding of the adiabatic shear phenomenon. From the viewpoint of a metallurgist, this might be a desirable circumstance. Rather than the heat capacity, temperature dependence of flow stress, and strain hardening capacity as the only important variables, an essential role of these fracture-related processes would mean that aspects of microstructure more amenable to metallurgical influence could have a decisive influence on the strain localization process.

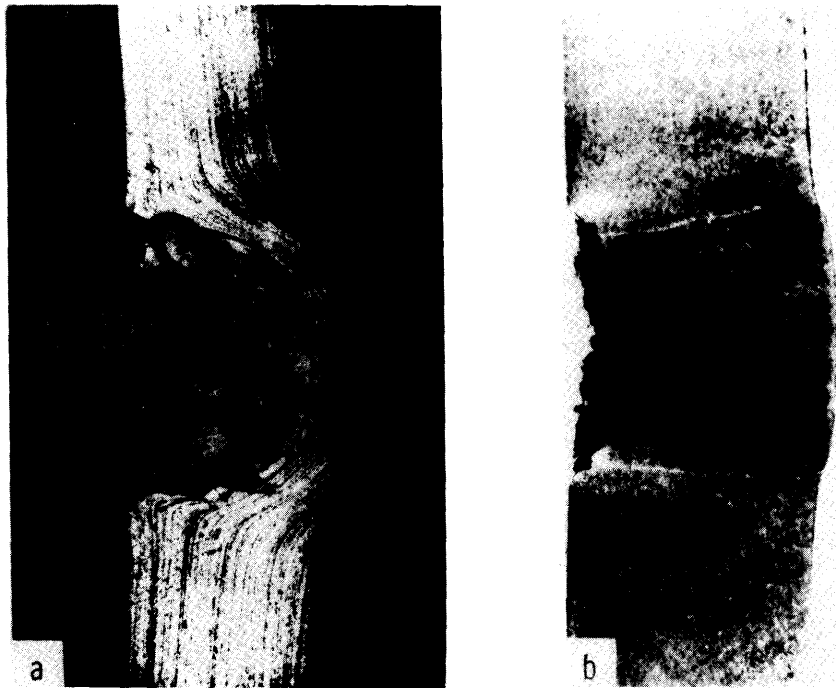


Figure 1. Penetration of 0.22-inch (0.56 cm) 4340 steel plates by 0.22-inch-diameter flat-ended steel projectiles. a) HRC 15 target hardness, $v = 8.1 \times 10^4$ cm/s; b) HRC 52 target hardness, $v = 7.3 \times 10^4$ cm/s. (2)

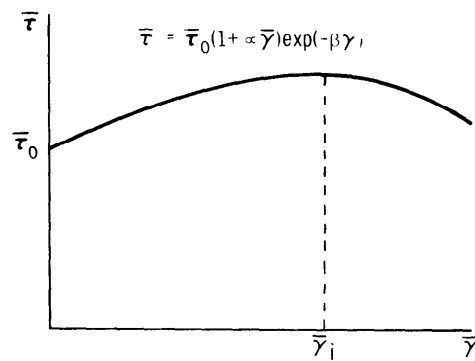


Figure 2. Schematic adiabatic stress-strain curve.

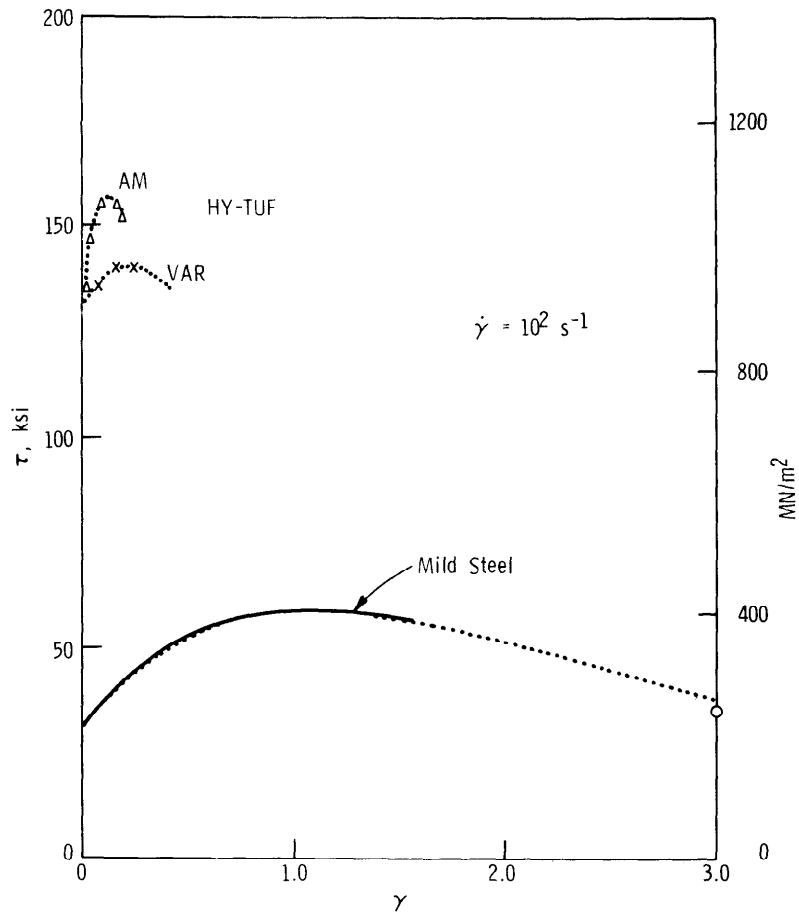


Figure 3. Fit of Eq. 5 to adiabatic torsion test results for mild steel and high-strength HY-TUF steel.

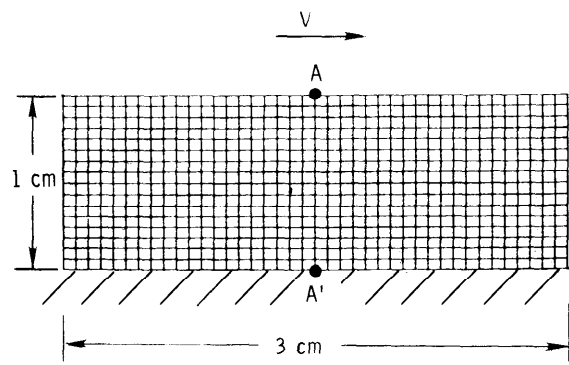


Figure 4. Grid pattern of rectangular body deformed in simple shear simulations.

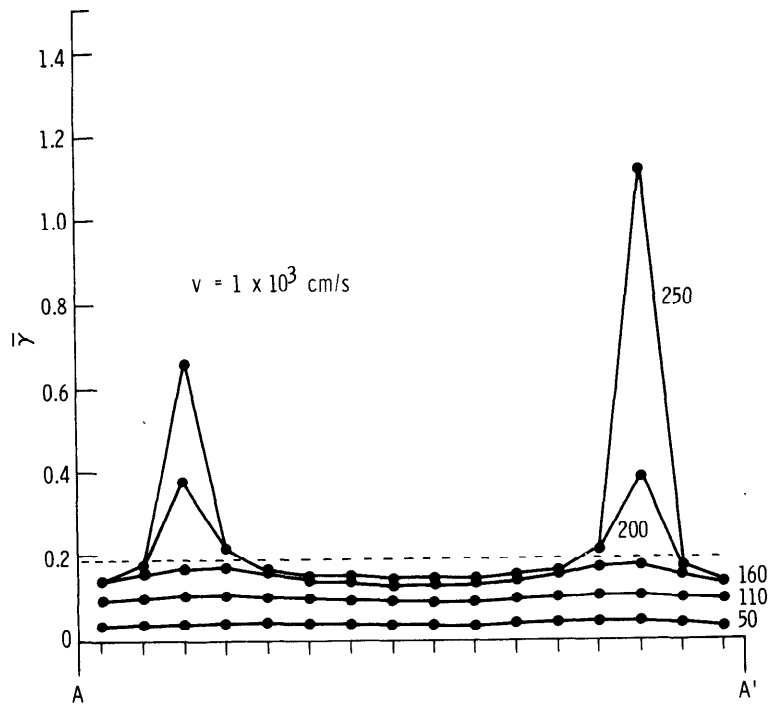


Figure 5. Strain profiles along AA' for $v = 1 \times 10^3$ cm/s.
Time expressed in microseconds.

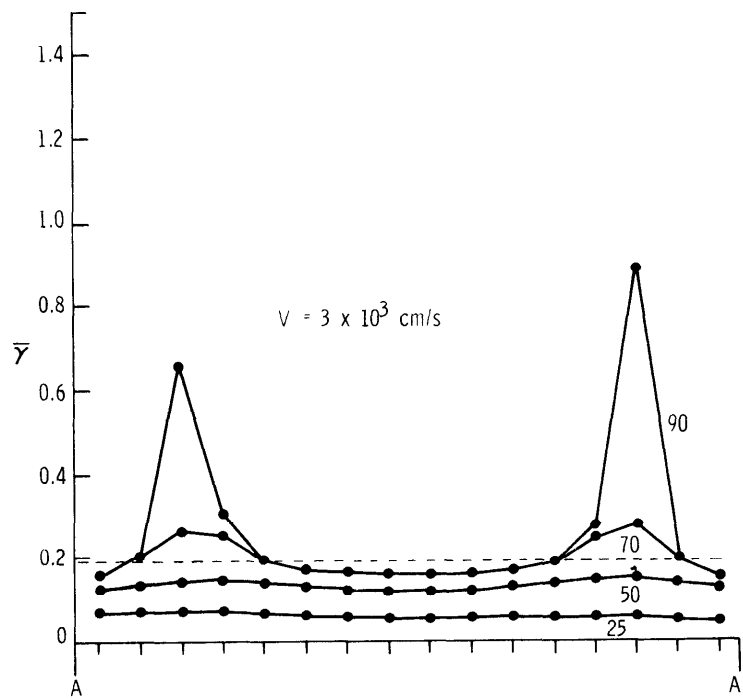


Figure 6. Strain profiles along AA' for $v = 3 \times 10^3$ cm/s.
Time expressed in microseconds.

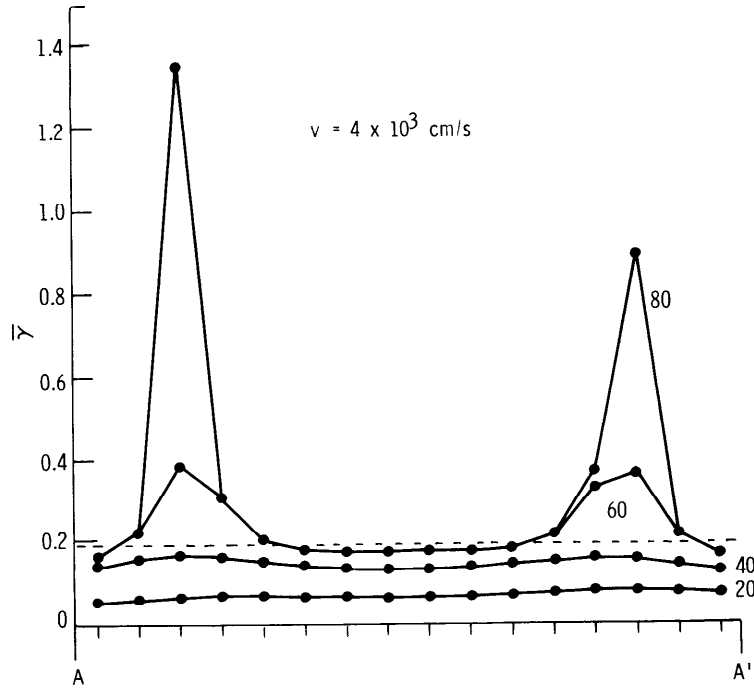


Figure 7. Strain profiles along AA' for $v = 4 \times 10^3 \text{ cm/s}$.
Time expressed in microseconds.

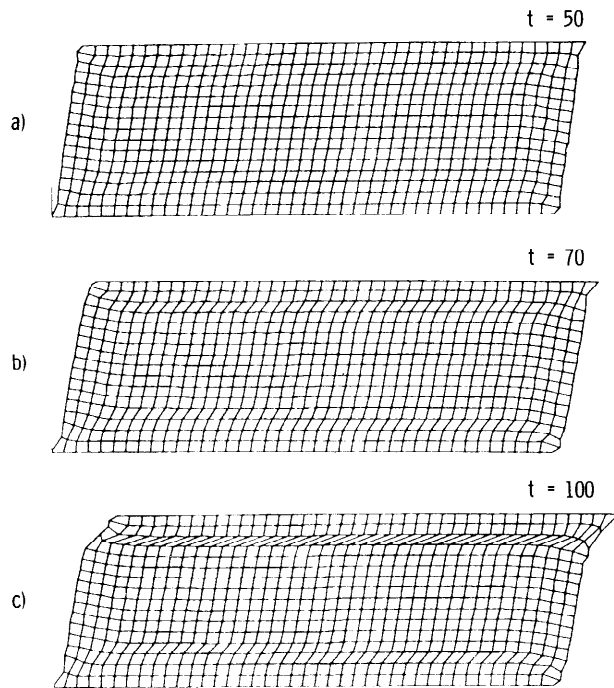


Figure 8. Grid pattern development with time
(in microseconds), $v = 4 \times 10^3 \text{ cm/s}$.

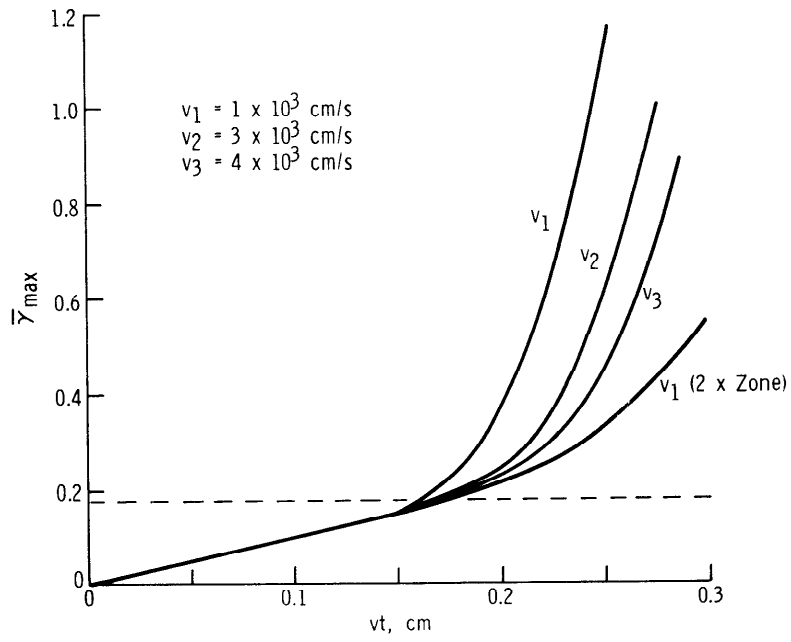


Figure 9. Maximum strain in AA' section versus imposed boundary displacement, vt.

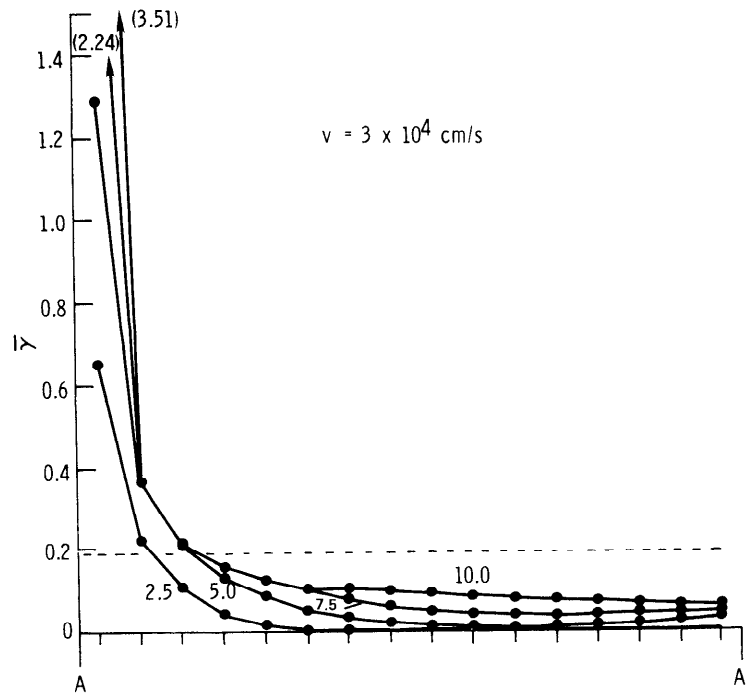


Figure 10. Strain profiles along AA' for $v = 3 \times 10^4 \text{ cm/s}$. Time expressed in microseconds.

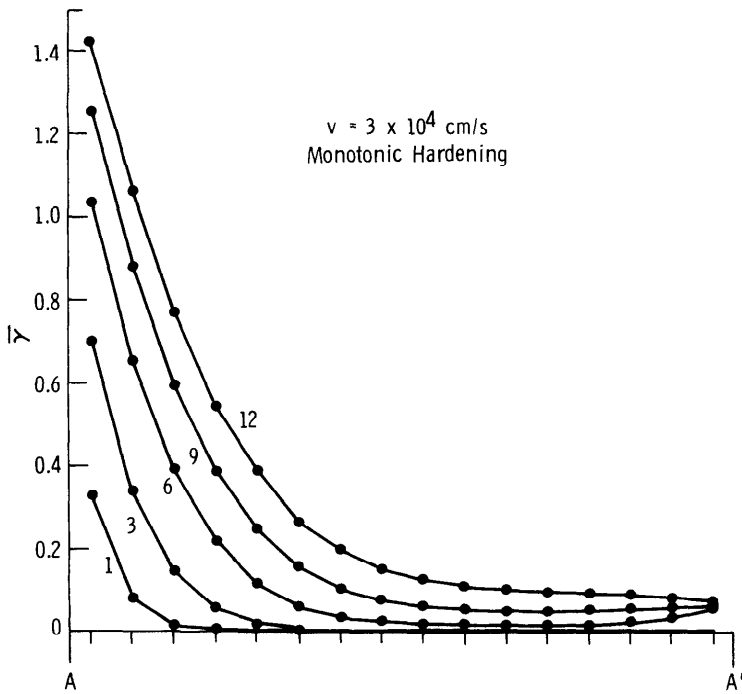


Figure 11. Strain profiles along AA' for $v = 3 \times 10^4 \text{ cm/s}$ with monotonic work hardening behavior. Time expressed in microseconds.

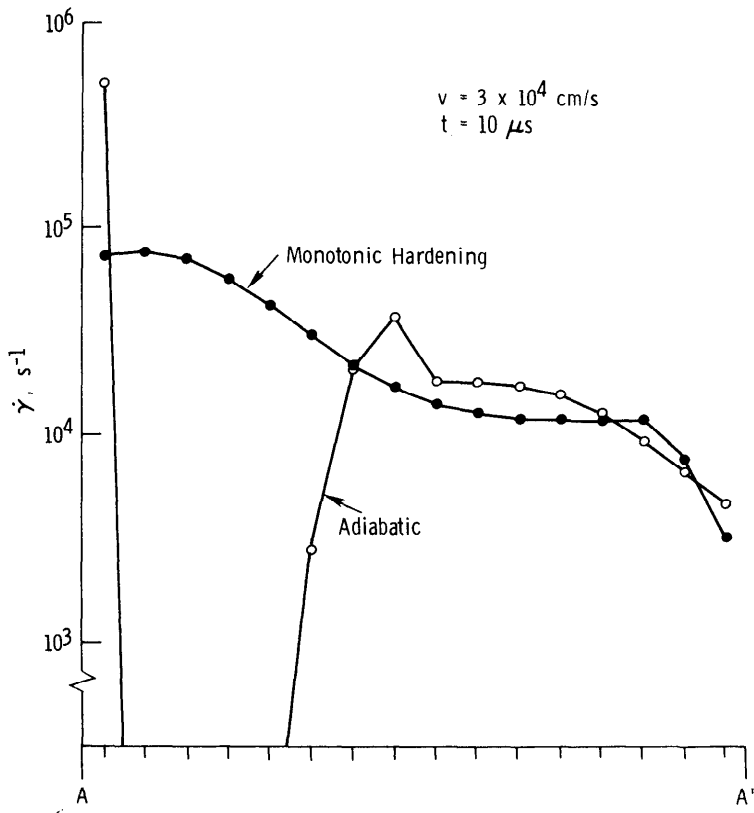


Figure 12. Local strain rate along AA' at $t = 10 \mu\text{s}$ for $v = 3 \times 10^4 \text{ cm/s}$ comparing monotonic hardening and adiabatic flow behavior.

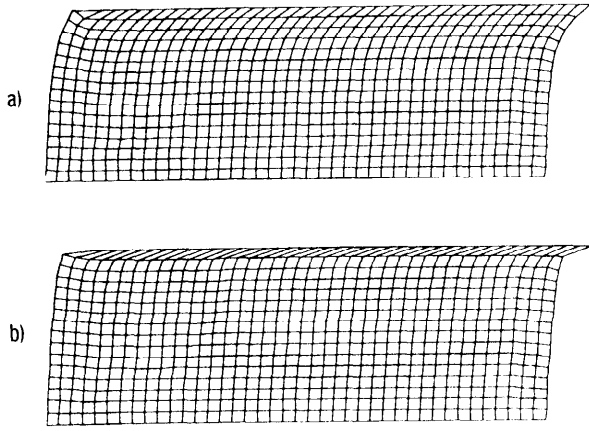


Figure 13. Comparison of complete grid patterns at $t = 10 \mu s$ for $v = 3 \times 10^4 \text{ cm/s}$.
a) monotonic hardening; b) adiabatic behavior.

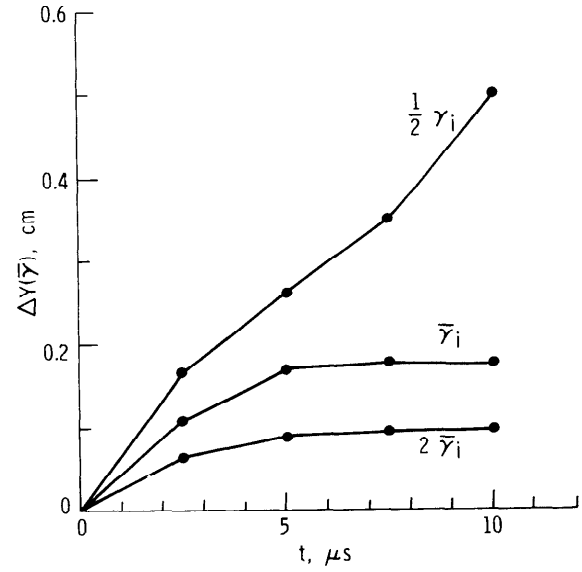


Figure 14. Position of constant strain contours with time for adiabatic flow behavior at $v = 3 \times 10^4 \text{ cm/s}$.

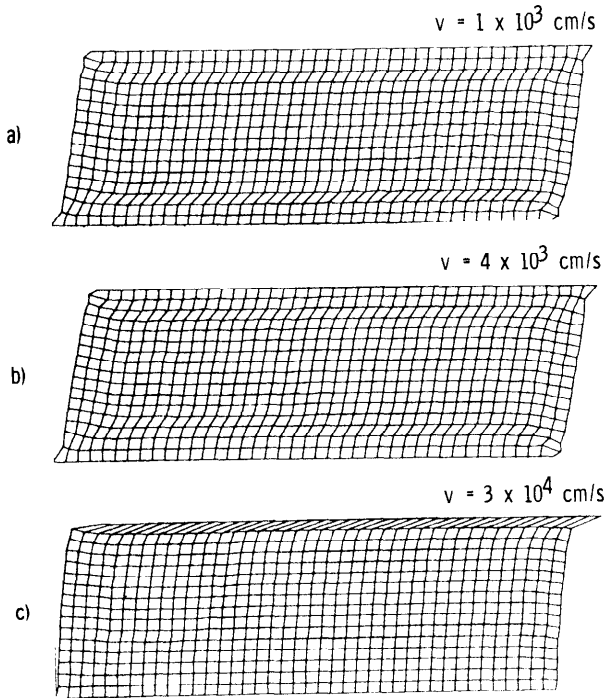


Figure 15. Effect of imposed boundary velocity on deformation pattern at comparable boundary displacements.

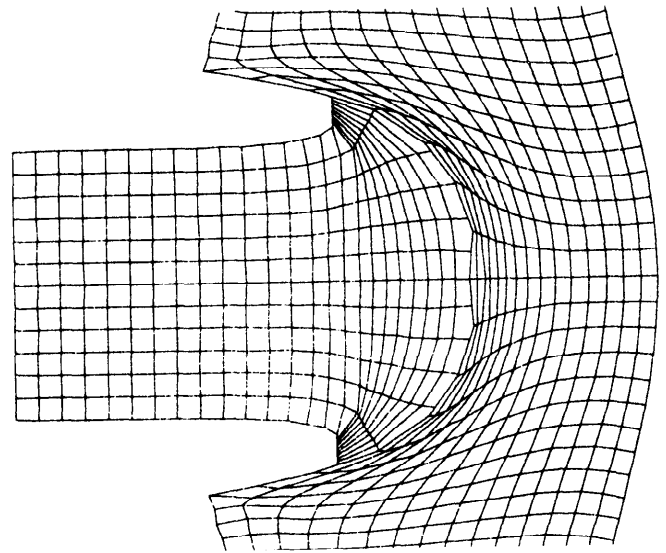


Figure 16. Simulation of ballistic penetration of mild steel plate by flat-ended high-strength steel projectile using adiabatic flow relations. Projectile velocity $7.5 \times 10^4 \text{ cm/s}$, $t = 20 \mu s$.

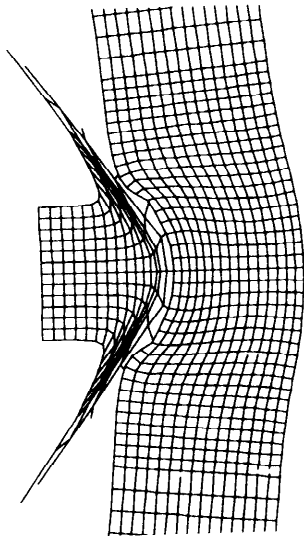


Figure 17. Simulation of impact of high-strength steel projectile on high-strength steel plate, projectile velocity 1.0×10^5 cm/s, $t = 35 \mu\text{s}$.

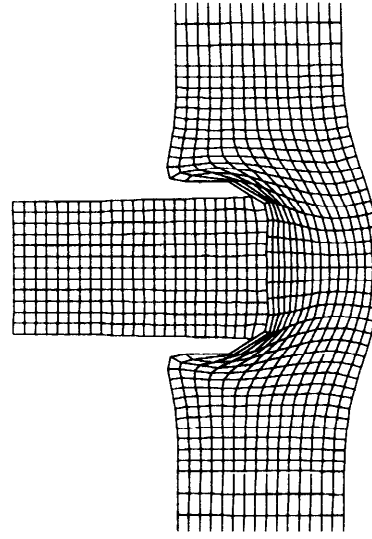


Figure 18. Simulation of ballistic penetration of high-strength steel plate by ultra-high strength steel projectile. Projectile velocity 1.0×10^5 cm/s, $t = 12 \mu\text{s}$.

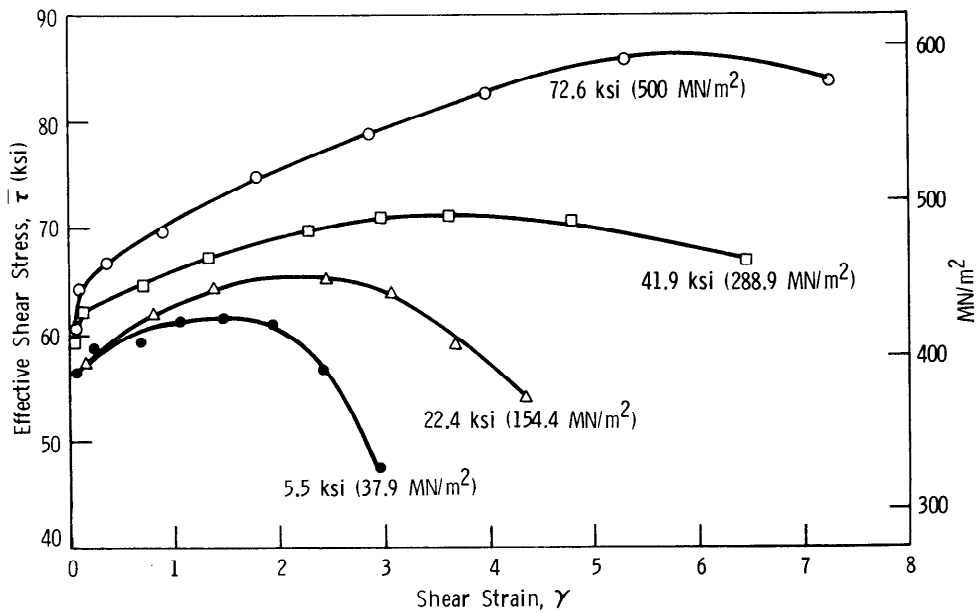


Figure 19. Effective shear stress-strain curves at indicated constant compressive stresses, mild steel.¹³

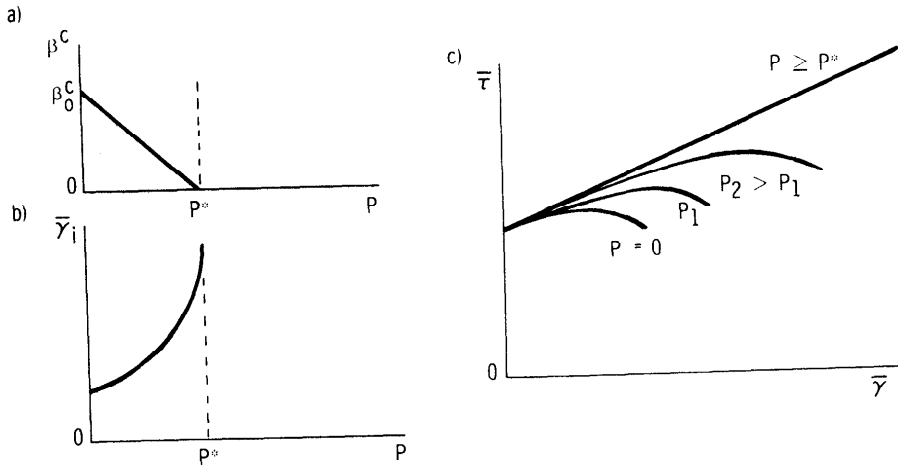


Figure 20. Schematic pressure-dependent behavior of β , γ_i , and $\bar{\tau}$ - $\bar{\gamma}$ curves for isothermal deformation with microcrack softening.

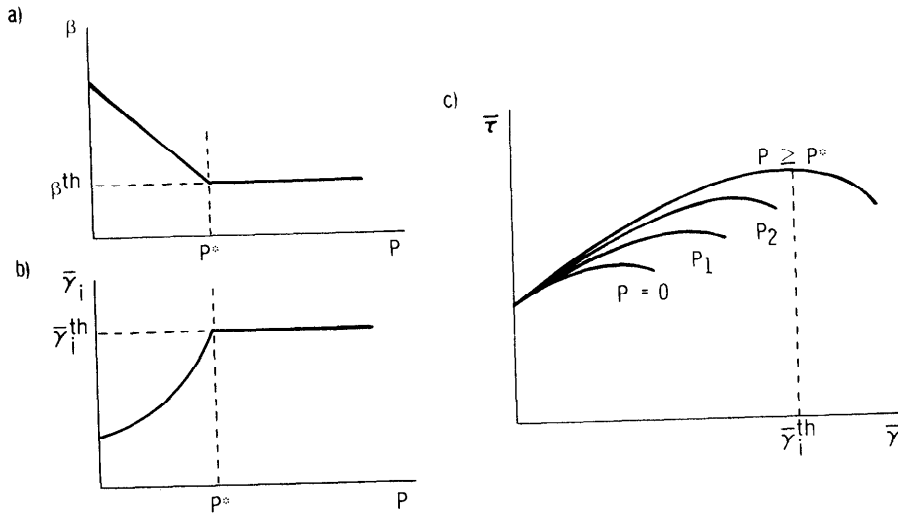


Figure 21. Schematic pressure-dependent behavior of β , γ_i , and $\bar{\tau}$ - $\bar{\gamma}$ curves for adiabatic deformation with both microcrack and thermal softening.

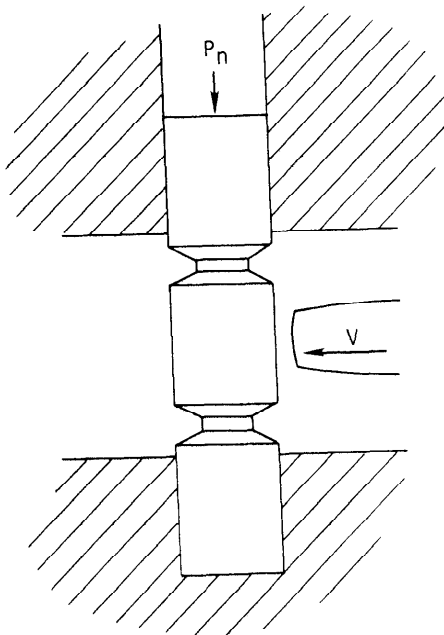


Figure 22. Configuration of adiabatic double shear + compression test to be applied to high-strength steels.

APPENDIX. ADIABATIC STRESS-STRAIN RELATIONS

The thermal softening effect represented by Eq. 1 can be expressed as:

$$\frac{\partial T}{\partial \bar{\gamma}} \frac{\partial \bar{\tau}}{\partial T} = -\beta \bar{\tau} \quad (\text{A-1})$$

with β given by

$$\beta = - \frac{f}{\rho C_p} \frac{\partial \bar{\tau}}{\partial T}. \quad (\text{A-2})$$

Taking β as a constant, the form of the adiabatic $\bar{\tau} - \bar{\gamma}$ curve at constant $\dot{\gamma}$ will depend on the form of the structural strain hardening behavior. A form commonly employed to describe isothermal strain hardening behavior is the simple power law hardening relation:

$$\bar{\tau} = K \bar{\gamma}^{-n} \quad (\text{A-3})$$

with K and n constants. This hardening behavior can be expressed in differential form as:

$$\frac{d\bar{\tau}}{d\bar{\gamma}} = n K \bar{\gamma}^{-n-1}, \quad (\text{A-4})$$

or, by substitution of Equation A-3,

$$\frac{d\bar{\tau}}{d\bar{\gamma}} = n \frac{\bar{\tau}}{\bar{\gamma}}. \quad (\text{A-5})$$

While Eq. A-5 is perhaps less physically meaningful than Eq. A-4 as a basic hardening law, it is mathematically more convenient; adopting Eq. A-5 and adding the thermal softening term of Eq. A-1 yields a simple separable differential equation for adiabatic flow:

$$\frac{d\bar{\tau}}{d\bar{\gamma}} = \left(\frac{n}{\bar{\gamma}} - \beta \right) \bar{\tau}. \quad (\text{A-6})$$

Integration yields the relation

$$\bar{\tau} = K \bar{\gamma}^{-n} \exp(-\beta \bar{\gamma}). \quad (\text{A-7})$$

Similarly, adopting other simple forms for the structural hardening behavior, and expressing the hardening rate as a function of stress, leads to the simple relations given in Table A-1. Some properties of these relations are also given in the table. Expressing the equivalent uniaxial tensile stress and strain as $\bar{\sigma} = \sqrt{3}\bar{\tau}$ and $\bar{\epsilon} = \bar{\gamma}/\sqrt{3}$, the associated tensile necking strain $\bar{\epsilon}_n$ is also included.

Table A-1. ADIABATIC STRESS-STRAIN RELATIONS

Stress-strain relation:	$\bar{\tau} = K\bar{\gamma}^{-n} \exp(-\beta\bar{\gamma})$	$\bar{\tau} = K(\bar{\gamma}+\bar{\gamma}_0)^n \exp(-\beta\bar{\gamma})$	$\bar{\tau} = \bar{\tau}_0 (1+\alpha\bar{\gamma})^n \exp(-\beta\bar{\gamma})$
Differential form:	$\frac{d\bar{\tau}}{d\bar{\gamma}} = \left(\frac{n}{\bar{\gamma}} - \beta\right) \bar{\tau}$	$\frac{d\bar{\tau}}{d\bar{\gamma}} = \left(\frac{n}{\bar{\gamma}+\bar{\gamma}_0} - \beta\right) \bar{\tau}$	$\frac{d\bar{\tau}}{d\bar{\gamma}} = \left(\frac{n\alpha}{1+\alpha\bar{\gamma}} - \beta\right) \bar{\tau}$
Yield stress:	-	$\bar{\tau}_y = K\bar{\gamma}_0^{-n}$	$\bar{\tau}_y = \bar{\tau}_0$
Tensile necking strain:	$\bar{\epsilon}_n = \frac{n}{\sqrt{3\beta+1}}$	$\bar{\epsilon}_n = \frac{n}{\sqrt{3\beta+1}} - \frac{\bar{\gamma}_0}{\sqrt{3}}$	$\bar{\epsilon}_n = \frac{n}{\sqrt{3\beta+1}} - \frac{1}{\sqrt{3\alpha}}$
Shear instability strain:	$\bar{\gamma}_i = \frac{n}{\beta}$	$\bar{\gamma}_i = \frac{n}{\beta} - \bar{\gamma}_0$	$\bar{\gamma}_i = \frac{n}{\beta} - \alpha^{-1}$
Maximum flow stress:	$\bar{\tau}_m = K\left(\frac{n}{\beta e}\right)^n$	$\bar{\tau}_m = K\left(\frac{n}{\beta e}\right)^n \exp(\beta\bar{\gamma}_0)$	$\bar{\tau}_m = \bar{\tau}_0 \left(\frac{n\alpha}{\beta e}\right)^n \exp\left(\frac{\beta}{\alpha}\right)$

Comparison with experimental results as in Figure 3 suggests that the third relation in Table A-1, with $n = 1$, is adequate for describing the behavior of high strength steels. This gives the relation of Eq. 5. The $\bar{\tau}_0$, α , and β parameters can be determined from the stress maximum point $\bar{\tau}_m$ ($\bar{\gamma}_i$) and one other point. Using the yield point, the ratio $r = \beta/\alpha$ can be obtained from

$$\ln \frac{\bar{\tau}_m}{\bar{\tau}_0} + 1 = r - \ln r. \quad (\text{A-8})$$

This is most easily determined from a plot of the function $x - \ln x$ versus x , as given in Figure A-1. From this r value, β and α are simply obtained by the relations

$$\beta = \frac{1-r}{\bar{\gamma}_i} \quad (\text{A-9})$$

and

$$\alpha = \beta/r. \quad (\text{A-10})$$

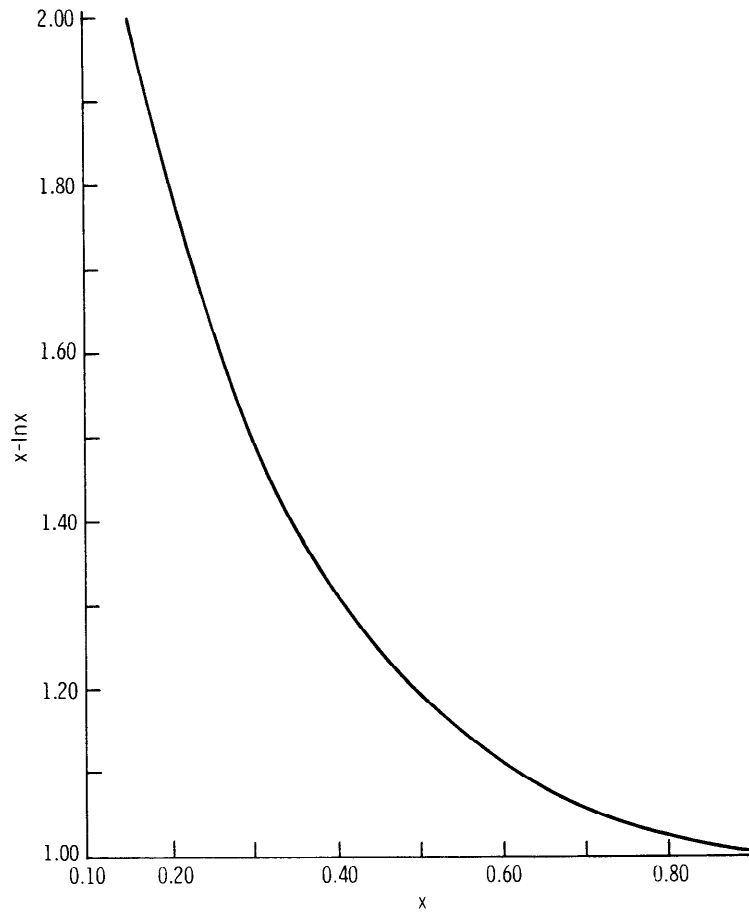


Figure A-1. Plot of $x-1nx$ versus x for fitting of Equation 5.

If the yield point is not well defined, another flow stress point $\bar{\tau}_1(\bar{\gamma}_1)$ can be used through the relation

$$\ln \frac{\bar{\tau}_m}{\bar{\tau}_1} + 1 = \eta - \ln \eta \quad (\text{A-11})$$

with

$$r = \frac{\eta - \frac{\bar{\gamma}_1}{\bar{\gamma}_i}}{1 - \frac{\bar{\gamma}_1}{\bar{\gamma}_i}} \quad (\text{A-12})$$

and α and β are again determined from r and $\bar{\gamma}_i$ through Equations A-9 and A-10.

ACKNOWLEDGMENTS

The authors are grateful to Ms. Anna M. Hansen for her assistance in running the computer simulations. Helpful discussion with Professor F. A. McClintock of M.I.T., particularly regarding slip-line-field solutions, is also appreciated. This work was performed at the Army Materials and Mechanics Research Center (AMMRC) as part of an ongoing program on adiabatic deformation and ballistic penetration.

LITERATURE CITED

1. ZENER, C., and HOLLOWOM, J. H. *Effect of Strain Rate Upon Plastic Flow of Steel*. J. Appl. Phys., v. 15, 1944, p. 22-32.
2. MESCALL, J., and PAPIRNO, R. *Spallation in Cylinder-Plate Impact*. Exp. Mech., v. 14, no. 7, 1974, p. 257-266.
3. ROGERS, H. C. *Adiabatic Shearing: A Review*. Drexel University Report prepared for U.S. Army Research Office, 1974.
4. ROGERS, H. C. *Adiabatic Plastic Deformation*. Ann. Rev. Mater. Sci., v. 9, 1979, p. 283-311.
5. BEDFORD, A. J., WINGROVE, A. L., and THOMPSON, K. R. L. J. Aust. Inst. Metals, v. 19, no. 1, 1974, p. 61-74.
6. CLIFTON, R. J. *Adiabatic Shear Banding in Materials Response to Ultra High Loading Rates*, Chap. 8, National Materials Advisory Board Committee, Rep. No. NMAB-356, 1980, p. 129-142.
7. ARGON, A. S. *Stability of Plastic Deformation in The Inhomogeneity of Plastic Deformation*, Chap. 7, ASM, Metals Park, OH, 1973, p. 161-189.
8. SAMUELS, L. E., and LAMBORN, I. R. *Failure Analysis of Armament Hardware in Metallography in Failure Analysis*. J. L. McCall and P. M. French, ed., Plenum Press, NY, 1978, p. 167-190.
9. CULVER, R. S. *Thermal Instability Strain in Dynamic Plastic Deformation in Metallurgical Effects at High Strain Rates*. R. W. Rohde, B. M. Butcher, J. R. Holland, and C. H. Karnes, ed., Plenum Press, NY, 1973, p. 519-530.
10. COSTIN, L. S., CRISMAN, E. E., HAWLEY, R. H., and DUFFY, J. *On the Localization of Plastic Flow in Mild Steel Tubes Under Dynamic Torsional Loading*, Brown University, Rep. No. NSF 18532/7, 1979.
11. LINDHOLM, U. S., and HARGREAVES, C. R. *Dynamic Testing of High Strength Steels and Their Susceptibility to Inhomogeneous Shear* in Proc. Second Int'l. Conf. on Mech. Beh. of Materials, ASM, Metals Park, OH, 1976, p. 1463-1467.
12. HARGREAVES, C. R., and HOEGFELDT, J. M. *The Effect of Strain Rate (Thermal Feedback) on the Deformation and Fracture Processes* in Proc. Second Int'l. Conf. on Mech. Beh. of Materials, ASM, Metals Park, OH, 1976, p. 1806-1810.
13. WALKER, T. J., and SHAW, M. C. *On Deformation at Large Strains in Advances in Machine Tool Design and Research*, S. A. Tobias, and F. Koenigsberger, ed., Pergamon Press, NY, 1969, p. 241-252.
14. LUONG, H. S. *A Study of Microvoid Formation in Metal Cutting*. PhD Thesis, Monash University, Victoria, Australia, 1977.
15. LUONG, H. S. *Discontinuities and Their Effects on Work Material in Chip Formation* in Proc. of Australian Conf. on Manufacturing Engineering, Monash University, Victoria, Australia, 1977, p. 122-126.
16. WOODWARD, R. L., and AGHAM, R. L. *The Structure of a White Etching Band in an Explosively Fractured Steel*. Metals Forum, v. 1, no. 4, 1978, p. 180-184.
17. TURLEY, D. M. *The Nature of the White Etching Surface Layers Produced During Reaming Ultra-High Strength Steel*. Mater. Sci. Engr., v. 19, 1975, p. 79-86.
18. WINGROVE, A. L. *A Note on the Structure of Adiabatic Shear Bands in Steel*. J. Aust. Inst. Metals, v. 16, no. 1, 1971, p. 67-70.
19. TRENT, E. M. *The Formation and Properties of Martensite on the Surface of Rope Wire*. J. Iron and Steel Inst., v. 143, no. 1, 1941, p. 401-419.
20. DeMORTON, M. E., and WOODWARD, R. L. *The Effect of Friction on the Structure of Surfaces Produced During Ballistic Tests*. Wear, v. 47, 1978, p. 195-209.
21. DOBROVOL'SKAYA, G. V., LEBEDEVA, I. L., and LYUBARASKIY, I. M. *Peculiarities of Friction Austenite*. Phys. Met. and Metall., v. 42, no. 5, 1976, p. 76-81.
22. BACKMAN, M. E., and FINNEGAN, S. A. *The Propagation of Adiabatic Shear in Metallurgical Effects at High Strain Rates*, R. W. Rohde, B. M. Butcher, J. R. Holland, and C. H. Karnes, ed., Plenum Press, NY, 1973, p. 531-543.
23. RUSSELL, R. J., and WINCHELL, P. G. *Reversal of Fe-Ni-C Martensite by Rapid Large Shear*. Met. Trans., v. 3, 1972, p. 2403-2409.
24. RECHT, R. F. *Catastrophic Thermoplastic Shear*. J. Appl. Mech., v. 86E, 1964, p. 189-193.
25. CARSLAW, H. S., and JAEGER, J. C. *Conduction of Heat in Solids*. Clarendon Press, Oxford, 1947.
26. CULVER, R. S. *Adiabatic Heating Effects in Dynamic Deformation* in Proc. Third Int'l. Conf. of Center for High Energy Forming, U. of Denver, CO, 1971, p. 4.3.1-4.3.38.
27. JEGLIC, F. S., and PACKWOOD, R. H. *Impact-Deposited White Layer on X65 Steel*. Metallography, v. 11, 1978, p. 43-50.
28. MANION, S. A., and STOCK, T. A. C. *The Measurement of Strain in Adiabatic Shear Bands*. J. Aust. Inst. Metals, v. 14, 1969, p. 190-191.
29. LEMAIRE, J. C., and BACKOFEN, W. A. *Adiabatic Instability in the Orthogonal Cutting of Steel*. Met. Trans., v. 3, 1972, p. 477-481.
30. YELLUP, J. M., and WOODWARD, R. L. *Investigations into the Prevention of Adiabatic Shear Failure in High Strength Armour Materials*. Res. Mechanica, v. 1, 1980, p. 41-57.
31. STOCK, T. A. C., and WINGROVE, A. L. *The Energy Required for High Speed Shearing of Steel*. J. Mech. Eng. Sci., v. 13, no. 2, 1971, p. 110-114.
32. ERLICH, D. C., CURRAN, D. R., and SEAM, L. *Further Development of a Computational Shear Band Model*. AMMRC TR 80-3, March 1980, SRI International Report prepared for Army Materials and Mechanics Research Center, Watertown, MA.
33. TSANGARAKIS, N. *Unpublished Research*. Army Materials and Mechanics Research Center, Watertown, MA.
34. WILKINS, M. L. *Calculation of Elastic-Plastic Flow*. Lawrence Radiation Lab., Livermore, CA, Rep. No. UCRL-7322, Rev. 1, 1969.
35. GREEN, A. P. *The Plastic Yielding of Metal Junctions Due to Combined Shear and Pressure*. J. Mech. Phys. Solids, v. 2, 1954, p. 197-211.
36. BRIDGMAN, P. W. *Studies in Large Plastic Flow and Fracture*. Chap. 15, Harvard University Press, Cambridge, MA, 1964, p. 247-278.
37. RUDNICKI, J. W., and RICE, J. R. *Conditions for the Localization of Deformation in Pressure-Sensitive Dilatant Materials*. J. Mech. Phys. Solids, v. 23, 1975, p. 371-394.
38. OLSON, G. B., and AZRIN, M. *Transformation Behavior of TRIP Steels*. Met. Trans., v. 9A, 1978, p. 713-721.
39. OLSON, G. B., and COHEN, M. *Stress-Assisted Isothermal Martensitic Transformation and Transformation Plasticity* in Proc. US/Japan Seminar on Mechanical Behavior of Metals and Alloys Associated with Displacive Phase Transformations, R. P. L., Troy, NY, 1979, p. 7.

DISTRIBUTION LIST

No. of Copies	To
1	Office of the Under Secretary of Defense for Research and Engineering, The Pentagon, Washington, DC 20301
12	Commander, Defense Technical Information Center, Cameron Station, Building 5, 5010 Duke Street, Alexandria, VA 22314
	Metals and Ceramics Information Center, Battelle Columbus Laboratories, 505 King Avenue, Columbus, OH 43201
1	ATTN: J. H. Brown, Jr.
1	Dr. Lee Semiatin
	Deputy Chief of Staff, Research, Development, and Acquisition, Headquarters, Department of the Army, Washington, DC 20301
1	ATTN: DAMA-ARZ
	Deputy Chief of Staff, Research, Development, and Acquisition, Headquarters, Department of the Army, Washington, DC 20301
1	ATTN: DAMA-ARZ
	Commander, Army Research Office, P.O. Box 12211, Research Triangle Park, NC 27709
1	ATTN: Information Processing Office
	Commander, U.S. Army Materiel Development and Readiness Command, 5001 Eisenhower Avenue, Alexandria, VA 22333
1	ATTN: DRCLDC
	Commander, U.S. Army Materiel Systems Analysis Activity, Aberdeen Proving Ground, MD 21005
1	ATTN: DRXSY-MP, Director
	Commander, U.S. Army Missile Command, Redstone Arsenal, AL 35809
1	ATTN: Technical Library
1	DRSMI-CS, R. B. Clem
	Commander, U.S. Army Armament Research and Development Command, Dover, NJ 07801
2	ATTN: Technical Library
1	DRDAR-SCM, J. D. Corrie
1	Dr. J. Waldman
	Commander, U.S. Army Tank-Automotive Command, Warren, MI 48090
1	ATTN: DRSTA-RKA
2	DRSTA-UL, Technical Library
1	DRSTA-RCK
	Commander, U.S. Army Foreign Science and Technology Center, 220 7th Street, N.E., Charlottesville, VA 22901
1	ATTN: Military Tech, Mr. Marley
	Director, Eustis Directorate, U.S. Army Air Mobility Research and Development Laboratory, Fort Eustis, VA 23604
1	ATTN: DAVDL-E-MOS
1	DAVDL-EU-TAP
	U.S. Army Aviation Training Library, Fort Rucker, AL 36360
1	ATTN: Building 5906--5907

No. of
Copies

To

Commander, U.S. Army Aviation Research and Development Command,
4300 Goodfellow Boulevard, St. Louis, MO 63120

1 ATTN: DRDAV-EGX
1 DRDAV-EX, Mr. R. Lewis
1 DRDAV-EQ, Mr. Crawford
1 DRCPM-AAH-TM, Mr. R. Hubbard
1 DRDAV-DS, Mr. W. McClane

Naval Research Laboratory, Washington, DC 20375

1 ATTN: Dr. J. M. Krafft - Code 5830
1 Code 2627

Chief of Naval Research, Arlington, VA 22217

1 ATTN: Code 471

Director, Structural Mechanics Research, Office of Naval Research,
800 North Quincy Street, Arlington, VA 22203

1 ATTN: Dr. N. Perrone

Commander, U.S. Air Force Wright Aeronautical Laboratories,
Wright-Patterson Air Force Base, OH 45433

2 ATTN: AFWAL/MLSE, E. Morrissey
1 AFWAL/MLC
1 AFWAL/MLLP, D. M. Forney, Jr.
1 AFWAL/MLBC, Mr. Stanley Schulman
1 AFWAL/MLXE, A. Olevitch

National Aeronautics and Space Administration, Washington, DC 20546

1 ATTN: Mr. B. G. Achhammer
1 Mr. G. C. Deutsch - Code RW

National Aeronautics and Space Administration, Marshall Space Flight
Center, Huntsville, AL 35812

1 ATTN: R. J. Schwinghammer, EH01, Dir, M&P Lab
1 Mr. W. A. Wilson, EH41, Bldg. 4612

Chief of Naval Operations, Washington, DC 20350

1 ATTN: OP-987, Director

Aeronautical Systems Division (AFSC), Wright-Patterson Air Force Base,
OH 45433

1 ATTN: ASD/ENFEF, D. C. Wight
1 ASD/ENFTV, D. J. Wallick
1 ASD/XRHD, G. B. Bennett

Air Force Armament Laboratory, Eglin Air Force Base, FL 32542

1 ATTN: AFATL/DLYA, V. D. Thornton

Air Force Flight Dynamics Laboratory, Wright-Patterson Air Force Base, OH 45433

1 ATTN: AFFDL/FES, G. W. Ducker
1 AFFDL/FES, J. Hodges
1 AFFDL/TST, Library

Air Force Test and Evaluation Center, Kirtland Air Force Base, NM 87115

1 ATTN: AFTEC-JT

No. of
Copies

To

1 Armament Development and Test Center, Eglin Air Force Base, FL 32542
ATTN: ADTC/TS

1 NASA - Ames Research Center, Mail Stop 223-6, Moffett Field, CA 94035
ATTN: SC, J. Parker

1 NASA - Ames Research Center, Army Air Mobility Research and Development
Laboratory, Mail Stop 207-5, Moffett Field, CA 94035
ATTN: SAVDL-AS-X, F. H. Immen

1 NASA - Johnson Spacecraft Center, Houston, TX 77058
ATTN: JM6

1 ES-5

1 Naval Air Development Center, Warminster, PA 18974
ATTN: Code 063

1 Naval Air System Command, Department of the Navy, Washington, DC 20360
ATTN: AIR-03PAF

1 AIR-5203

1 AIR-5204J

1 AIR-530313

1 Naval Material Command, Washington, DC 20360
ATTN: MAT-0331

1 Naval Post Graduate School Monterey, CA 93948
ATTN: Code 57BP, R. E. Ball

1 Naval Surface Weapons Center, Dahlgren Laboratory, Dahlgren, VA 22448
ATTN: Code G-54, Mr. J. Hall

1 Code G-54, Mr. E. Rowe

1 Naval Weapons Center, China Lake, CA 93555
ATTN: Code 40701

1 Code 408

1 Commander, Rock Island Arsenal, Rock Island, IL 61299
ATTN: DRSAR-PPV

1 Armament Systems, Inc., 712-F North Valley, Anaheim, CA 92801
ATTN: J. Musch

1 Beech Aircraft Corporation, 9709 E. Central Avenue, Wichita, KS 67206
ATTN: Engineering Library

1 Bell Helicopter Company, A Textron Company, P.O. Box 482,
Fort Worth, TX 76101
ATTN: J. R. Johnson

1 Boeing Vertol Company, A Division of the Boeing Company, P.O. Box 16858,
Philadelphia, PA 19142
ATTN: J. E. Gonsalves, M/S P32-19

1 Calspan Corporation, P.O. Box 235, Buffalo, NY 14221
ATTN: Library

No. of
Copies

To

1 Cessna Aircraft Company, Wallace Division, P.O. Box 1977, Wichita, KS 67201
ATTN: B. B. Overfield

1 Fairchild Industries, Inc., Fairchild Republic Company, Conklin Street,
Farmingdale, Long Island, NY 11735
ATTN: Engineering Library, G. A. Mauter

1 Falcon Research and Development Company, 601 San Pedro, N.E., Suite 205,
Albuquerque, NM 87108
ATTN: W. L. Baker

1 General Dynamics Corporation, Convair Division, P.O. Box 80877,
San Diego, CA 92138
ATTN: Research Library, U. J. Sweeney

1 General Research Corporation, Science and Technology Division,
5383 Hollister Avenue, P.O. Box 3587, Santa Barbara, CA 93105
ATTN: R. Rodman

1 Gruman Aerospace Corporation, South Oyster Bay Road, Bethpage, NY 11714
ATTN: Technical Information Center, J. Davis

1 Hughes Helicopters, A Division of Summa Corporation, Centinela & Teale Street,
Culver City, CA 90230
ATTN: Library, 2/T2124, D. K. Goss
Mr. A. Hirko
Mr. L. Soffa
Mr. A. Edwards

1 IIT Research Institute, 10 West 35th Street, Chicago, IL 60616
ATTN: K. McKee

1 Kaman Aerospace Corporation, Old Winsor Road, Bloomfield, CT 06002
ATTN: H. E. Showalter

1 Lockheed-California Company, A Division of Lockheed Aircraft Corporation, Burbank,
CA 91503
ATTN: Technological Information Center, 84-40, U-35, A-1

1 Vought Corporation, P.O. Box 5907, Dallas, TX 75232
ATTN: D. M. Reedy, 2-30110
M. P. Poulos, Jr.

1 Martin Marietta Corporation, Orlando Division, P.O. Box 5837, Orlando, FL 32805
ATTN: Library, M. C. Griffith

1 McDonnell Douglas Corporation, 3855 Lakewood Boulevard, Long Beach, CA 90846
ATTN: Technical Library, CI 290/36-84

1 Northrop Corporation, Aircraft Division, 3901 W. Broadway, Hawthorne, CA 90250
ATTN: Mgr. Library Services, H. W. Jones

1 Parker Hannifin Corporation, Bertea Control Systems Division,
18001 Von Karman Avenue, Irvine, CA 92715
ATTN: C. Beneker

1 Rockwell International Corporation, Los Angeles Aircraft Division,
B-1 Division, International Airport, Los Angeles, CA 90009
ATTN: W. L. Jackson

No. of
Copies

To

Rockwell International Corporation, Science Center, 1049 Camino Dos Rios,
Thousand Oaks, CA 91360
1 ATTN: Dr. Neal E. Paton
1 Dr. Amit K. Ghosh

Sikorsky Aircraft, A Division of United Aircraft Corporation, Main Street,
Stratford, CT 06602
1 ATTN: J. B. Faulk
1 W. G. Degnan

Teledyne CAE, 1330 Laskey Road, Toledo, OH 43697
1 ATTN: Librarian, M. Dowdell

Simonds Steel Division, Guterl Special Steel Corporation, Lockport, NY 14094
1 ATTN: Mr. R. Farrington

Atlas Testing Laboratories, Inc., 6929 E. Slauson Avenue, Los Angeles, CA 90040
1 ATTN: Mr. P. S. Horvath

Georgia Institute of Technology, School of Mechanical Engineering,
Atlanta, GA 30332
1 ATTN: Dr. J. T. Berry

Lukens Steel Company, Coatesville, PA 19320
1 ATTN: Dr. R. S. Swift

Republic Steel Corporation, 410 Oberlin Avenue SW, Massillon, OH 44646
1 ATTN: Mr. R. Sweeney
1 Mr. W. H. Brechtel
1 Mr. B. G. Hughes

Boeing Commercial Airplane Company, P.O. Box 3707, MS73-43, Seattle, WA 98124
1 ATTN: Dr. K. White

United States Steel Corporation, Research Laboratory, Monroeville, PA 15146
1 ATTN: Dr. Hsun Hu

METTEC, 1805 E. Carnegie Avenue, Santa Ana, CA 92705
1 ATTN: Dr. L. Raymond

Cabot Corporation, Machinery Division, P.O. Box 1101, Pampa, TX 79065
1 ATTN: Mr. W. L. Hallerberg

Brown University, Division of Engineering, Providence, RI 02912
1 ATTN: Prof. J. Duffy
1 Prof. R. Clifton

SRI International, 333 Ravenswood Avenue, Menlo Park, CA 94025
1 ATTN: Dr. D. Shockey

Harvard University, Division of Applied Science, Cambridge, MA 02138
1 ATTN: Prof. B. Budiansky
1 Prof. J. Hutchinson

Honeywell, Inc., Defense Systems Division, 600 Second Street, N.E.,
Hopkins, Minnesota 55343
1 ATTN: Mr. Charles R. Hargreaves

No. of
Copies

To

Massachusetts Institute of Technology, Department of Mechanical Engineering,
Room 1-306, Cambridge, MA 02139
1 ATTN: Prof. Ali S. Argon

Drexel University, Department of Materials Engineering, Philadelphia, PA 19104
1 ATTN: Prof. Harry C. Rogers

Arizona State University, College of Engineering and Applied Sciences,
Tempe, AZ 85281
1 ATTN: Prof. Milton C. Shaw

Syracuse University, 304 Administration Building, Syracuse, NY 13210
1 ATTN: Prof. Volker Weiss

Sandia Laboratories, Division 5532, Albuquerque, NM 87115
1 ATTN: Dr. L. S. Costin

Director, Army Materials and Mechanics Research Center, Watertown, MA 02172
2 ATTN: DRXMR-PL
3 Authors

Army Materials and Mechanics Research Center,
Watertown, Massachusetts 02172
ADIABATIC DEFORMATION AND STRAIN
LOCALIZATION - Gregory B. Olson,
John F. Mescall, and Morris Azrin

AD
UNCLASSIFIED
UNLIMITED DISTRIBUTION
Key Words

Technical Report AMMRC TR 82-48, August 1982, 28 pp -
illus-tables, D/A Project 1L161102AH42,
AMCMS Code 611102.H420011

Adiabatic flow
Shear flow
Ballistics

The strain localization phenomenon of "adiabatic shear" is generally attributed to a plastic instability arising from a thermal softening effect during adiabatic or near-adiabatic plastic deformation. High strain-rate adiabatic torsion tests indicate that the effective shear stress-strain ($\bar{\tau}$ - $\bar{\gamma}$) relations for high-strength (rate-insensitive) steels can be described by a simple expression of the form:

$$\bar{\tau} = \bar{\tau}_0 (1 + \alpha \bar{\gamma}) \exp(-\beta \bar{\gamma})$$

where $\bar{\tau}_0$ is a constant, α and β are dimensionless hardening and softening parameters. The flow stress reaches a maximum at an instability strain, $\bar{\gamma}_i = \beta^{-1} \alpha^{-1}$. With parameters derived from the torsion tests, this relation has been used in computer simulations of the development of intense shear localization in a simple uniformly loaded body. Strain localization has been studied under conditions of both quasistatic and dynamic deformation. Application to the simulation of ballistic penetration is in progress. Experimental evidence indicates the existence of a pressure-dependent strain softening effect attributed to subcritical shear microcracks which contributes to shear instability in mild steels. This phenomenon may also operate in high-strength steels, giving rise to a pressure-dependent β parameter. Experiments are being designed to determine the relative importance of this effect in the adiabatic deformation of high-strength steels and its possible role in ballistic penetration.

Army Materials and Mechanics Research Center,
Watertown, Massachusetts 02172
ADIABATIC DEFORMATION AND STRAIN
LOCALIZATION - Gregory B. Olson,
John F. Mescall, and Morris Azrin

AD
UNCLASSIFIED
UNLIMITED DISTRIBUTION
Key Words

Technical Report AMMRC TR 82-48, August 1982, 28 pp -
illus-tables, D/A Project 1L161102AH42,
AMCMS Code 611102.H420011

Adiabatic flow
Shear flow
Ballistics

The strain localization phenomenon of "adiabatic shear" is generally attributed to a plastic instability arising from a thermal softening effect during adiabatic or near-adiabatic plastic deformation. High strain-rate adiabatic torsion tests indicate that the effective shear stress-strain ($\bar{\tau}$ - $\bar{\gamma}$) relations for high-strength (rate-insensitive) steels can be described by a simple expression of the form:

$$\bar{\tau} = \bar{\tau}_0 (1 + \alpha \bar{\gamma}) \exp(-\beta \bar{\gamma})$$

where $\bar{\tau}_0$ is a constant, α and β are dimensionless hardening and softening parameters. The flow stress reaches a maximum at an instability strain, $\bar{\gamma}_i = \beta^{-1} \alpha^{-1}$. With parameters derived from the torsion tests, this relation has been used in computer simulations of the development of intense shear localization in a simple uniformly loaded body. Strain localization has been studied under conditions of both quasistatic and dynamic deformation. Application to the simulation of ballistic penetration is in progress. Experimental evidence indicates the existence of a pressure-dependent strain softening effect attributed to subcritical shear microcracks which contributes to shear instability in mild steels. This phenomenon may also operate in high-strength steels, giving rise to a pressure-dependent β parameter. Experiments are being designed to determine the relative importance of this effect in the adiabatic deformation of high-strength steels and its possible role in ballistic penetration.

Army Materials and Mechanics Research Center,
Watertown, Massachusetts 02172
ADIABATIC DEFORMATION AND STRAIN
LOCALIZATION - Gregory B. Olson,
John F. Mescall, and Morris Azrin

AD
UNCLASSIFIED
UNLIMITED DISTRIBUTION
Key Words

Technical Report AMMRC TR 82-48, August 1982, 28 pp -
illus-tables, D/A Project 1L161102AH42,
AMCMS Code 611102.H420011

Adiabatic flow
Shear flow
Ballistics

The strain localization phenomenon of "adiabatic shear" is generally attributed to a plastic instability arising from a thermal softening effect during adiabatic or near-adiabatic plastic deformation. High strain-rate adiabatic torsion tests indicate that the effective shear stress-strain ($\bar{\tau}$ - $\bar{\gamma}$) relations for high-strength (rate-insensitive) steels can be described by a simple expression of the form:

$$\bar{\tau} = \bar{\tau}_0 (1 + \alpha \bar{\gamma}) \exp(-\beta \bar{\gamma})$$

where $\bar{\tau}_0$ is a constant, α and β are dimensionless hardening and softening parameters. The flow stress reaches a maximum at an instability strain, $\bar{\gamma}_i = \beta^{-1} \alpha^{-1}$. With parameters derived from the torsion tests, this relation has been used in computer simulations of the development of intense shear localization in a simple uniformly loaded body. Strain localization has been studied under conditions of both quasistatic and dynamic deformation. Application to the simulation of ballistic penetration is in progress. Experimental evidence indicates the existence of a pressure-dependent strain softening effect attributed to subcritical shear microcracks which contributes to shear instability in mild steels. This phenomenon may also operate in high-strength steels, giving rise to a pressure-dependent β parameter. Experiments are being designed to determine the relative importance of this effect in the adiabatic deformation of high-strength steels and its possible role in ballistic penetration.

Army Materials and Mechanics Research Center,
Watertown, Massachusetts 02172
ADIABATIC DEFORMATION AND STRAIN
LOCALIZATION - Gregory B. Olson,
John F. Mescall, and Morris Azrin

AD
UNCLASSIFIED
UNLIMITED DISTRIBUTION
Key Words

Technical Report AMMRC TR 82-48, August 1982, 28 pp -
illus-tables, D/A Project 1L161102AH42,
AMCMS Code 611102.H420011

Adiabatic flow
Shear flow
Ballistics

The strain localization phenomenon of "adiabatic shear" is generally attributed to a plastic instability arising from a thermal softening effect during adiabatic or near-adiabatic plastic deformation. High strain-rate adiabatic torsion tests indicate that the effective shear stress-strain ($\bar{\tau}$ - $\bar{\gamma}$) relations for high-strength (rate-insensitive) steels can be described by a simple expression of the form:

$$\bar{\tau} = \bar{\tau}_0 (1 + \alpha \bar{\gamma}) \exp(-\beta \bar{\gamma})$$

where $\bar{\tau}_0$ is a constant, α and β are dimensionless hardening and softening parameters. The flow stress reaches a maximum at an instability strain, $\bar{\gamma}_i = \beta^{-1} \alpha^{-1}$. With parameters derived from the torsion tests, this relation has been used in computer simulations of the development of intense shear localization in a simple uniformly loaded body. Strain localization has been studied under conditions of both quasistatic and dynamic deformation. Application to the simulation of ballistic penetration is in progress. Experimental evidence indicates the existence of a pressure-dependent strain softening effect attributed to subcritical shear microcracks which contributes to shear instability in mild steels. This phenomenon may also operate in high-strength steels, giving rise to a pressure-dependent β parameter. Experiments are being designed to determine the relative importance of this effect in the adiabatic deformation of high-strength steels and its possible role in ballistic penetration.